To probe the binding interactions between two FDA approved migraine drugs (Ubrogepant and Rimegepant) and calcitonin-gene related peptide receptor (CGRPR) using molecular dynamics simulations

Lauren Leung[3], Siyan Liao[1 2] and Chun Wu*[1 2]

[1] Key Laboratory of Molecular Target & Clinical Pharmacology, School of Pharmaceutical Sciences, Guangzhou Medical University, Guangzhou, 511436, China

[2] College of Science and Mathematics, Rowan University, Glassboro, NJ, 08028 USA

[3] College of Letters and Sciences, University of California, Santa Barbara, Santa Barbara, CA, 93107 USA

* Corresponding author
E-mail address: wuc@rowan.edu (Chun Wu).

Abstract

Recently, FDA approved ubrogepant and rimegepant as oral drugs to treat migraines by targeting the calcitonin-gene related peptide receptor (CGRPR). Unfortunately, there is no high-resolution complex structure with these two drugs, thus the detailed interaction between drugs and the receptor remains to be elusive. This study uses molecular docking and molecular dynamics simulation to model the drug-receptor complex and analyze their binding interactions at a molecular level. The complex crystal structure (3N7R) of the gepant drugs' predecessor, olcegepant, was used for our molecular docking of the two drugs and served as a control system. The three systems, with ubrogepant, rimegepant, crystal olcegepant, were subject to 3x1000ns molecular dynamics simulations and followed by the simulation interaction diagram (SID), the structural clustering and MM-GBSA binding energy analyses. Our MD data revealed that olcegepant binds most strongly to the CGRPR, followed by ubrogepant then rimegepant, largely due to changes in hydrophobic and electrostatic interactions. The order of our MM-GBSA binding energies of these three compounds is consistent with their experimental IC_{50} values. SID analysis revealed the pharmacophore of the gepant class to be the dihydroquinazolinone group. Subtle differences in interaction profile have been noted, including interactions with the W74 and W72 residues. The ubrogepant and rimegepant both contact A70 and M42 of the receptor, while olcegepant does not. The results of this study elucidate the interactions in the binding pocket of CGRP receptor and can assist in further development for orally available antagonists of the CGRP receptor.

Keywords: Ubrogepant; rimegepant; molecular dynamics simulation; MM-GBSA, CGRP/calcitonin gene receptor peptide, CLR/calcitonin-like receptor, RAMP/receptor-activity modifying protein

I. Introduction

According to a 2016 study, roughly 1.04 billion people experience migraines worldwide [1]. During a migraine, the level of the calcitonin gene related peptide (CGRP) hormone, a potent vasodilator, in the cranial blood circulation will rise [2]. The effectors of CGRPs are calcitonin gene related peptide receptors (CGRPR) which belong to class B secretin G-protein coupled receptors (GPCR) and has been a growing area of research in the development of anti-migraine drugs. Unfortunately, class B secretin receptors are especially difficult to crystallize and very few full crystal structures of class B receptors exist [3-6]. Like class A GPCRs, class B secretin receptors exhibit the typical seven transmembrane α-helices of GPCRs. Additionally, class B secretin receptors include a large N-terminal extracellular domain (ECD) [3-5, 7]. The class B of receptors includes the calcitonin (CT) receptor family with two members: the calcitonin receptor (CTR) and the calcitonin-like receptor (CLR). Both CTR and CLR are capable of dimerization with a specific transmembrane receptor activity modifying protein (RAMP 1-3) [4, 8-20]. These dimers are activated mainly by potent vasodilators. Specifically, the CLR/RAMP2 and CLR/RAMP1 dimers can be activated by adrenomedullin and CGRP, respectively [10, 11, 18, 20-23]. This study will focus on the CLR/RAMP1 complex which, upon binding of CGRP, will stimulate the G_s-protein complex and cause migraines (Figure S1) [24, 25].

The gepant class of drugs was developed to bind the CLR/RAMP1 receptor and act as an antagonist to the natural CLR/RAMP1. Previous drugs in the gepants class such as telcagepant and olcegepant were intravenously administered (Table 1). Telcagepant was discontinued in 2011 when studies showed compound-related adverse effects leading to hepatoxicity [26-28]. Olcegepant (IC_{50} = 0.030 nM) [21], on the other hand, showed to be a promising competitive inhibitor (Figure S1) [29]. However, difficulty in formulating orally administered olcegepant ultimately led to its discontinuation. Ubrogepant is the first in its class to orally treat migraines,

followed by rimegepant. Both are antagonists of the CLR/RAMP1 receptor and have recently been approved by the FDA to orally treat migraines. Ubrogepant is an orally available drug approved in 2019 [30, 31]. Rimegepant is an orally disintegrating tablet (ODT) approved in February 2020 [32, 33] and may be more effective than ubrogepant with respect to sustained pain freedom [34]. The administration of an orally disintegrating tablet may also help patients with dysphagia, the difficulty of swallowing. Ubrogepant has an experimental IC_{50} value of 0.08 nM [30, 35], and rimegepant has an IC_{50} value of 0.14 nM [32]. Both have low molecular weights that allow them to be orally bioavailable.

Liang et al has proposed a full length cryo-EM structure of the CGRP-agonist bound CLR/RAMP1 in complex with G-proteins (Figure S1) [24]. It was experimentally determined that the antagonist olcegepant would act as a competitive inhibitor to block the C-terminal of CGRP, thereby preventing activation of the G_s-protein complex and inhibiting increased cAMP levels [25, 29, 36-39]. The crystal structure of the ECD of the CLR/RAMP1 complex with olcegepant was solved by Ter Haar et al [40]. This structure shows olcegepant binding to the pocket interface between the characteristic ECD of the CLR and RAMP1 (Figure 1). The superimposition of the crystal ECD/RAMP1 structure and full-length cryo-EM structure show minimal interactions between the antagonist and the transmembrane domain or G-proteins (Figure S1). Thus, the transmembrane domain and G-proteins have been omitted from this study to reduce computational costs.

The crystal ECD/RAMP1 structure has been used to identify key binding interactions between the crystal ligand, olcegepant, and ECD/RAMP1 receptor [9, 10, 40]. However, no crystal structure has been solved for the newly FDA approved ubrogepant or rimegepant. This study will probe the interactions of ubrogepant and rimegepant in the binding pocket of the

ECD/RAMP1 receptor using molecular docking, molecular dynamics simulation with molecular mechanics generalized Born surface area (MM-GBSA) binding energy analysis. Understanding the interactions and energy dynamics within the binding pocket may help further drug design efforts for CLR/RAMP1 antagonists and mechanistic studies of the CLR/RAMP1 receptor.

II. Results and Discussion

ESOL method reveals solubility of rimegepant > ubrogepant > olcegepant. The SwissADME database was used to calculate water solubility of each ligand by the ESOL method [41] [42]. Results showed greatest solubility of rimegepant (logS = -6.40), followed by ubrogepant (logS = -5.14), then olcegepant (logS = -4.67) (Table 2).

Convergence of simulations was confirmed by RMSD analysis of protein and ligand. The root-mean squared deviation was calculated to measure the average change in displacement of the Cα backbone in the protein and heavy atoms in the ligand (Figure 2, Figure S2-4). The ligand and protein RMSD of the olcegepant-protein complex maintain a deviation of about 2.5±0.2 Å and 2.3±0.2 Å for protein and ligand, respectively. The ligand RMSD values for ubrogepant and rimegepant maintain an average RMSD of 0.8±0.1 Å and 1.0±0.1 Å, respectively, indicating that the induced fit poses of each complex appear to be stable. These values indicate that the ligand maintained its position and did not diffuse away from the binding pocket site. The protein RMSD of the ubrogepant-receptor complex remains relatively stable at an average RMSD of 2.4±0.3 Å during the simulation. The protein RMSD of rimegepant-receptor complex remains relatively stable at an average RMSD of 2.1±0.1 Å.

Trajectory clustering analysis reveals a single conformation like the initial pose of each

complex. Clustering analysis was performed on each system to group the frames into structure families. For each complex, only one structural family was generated, and its centroid structure was used for further analysis. Ligand superimposition of the three cluster representatives show conserved binding poses, specifically at the dihydroquinazolinone portion of olcegepant, the dihydropyrrolopyridinone of ubrogepant, and the dihydroimidazopyridinone of rimegepant (Figure S5). The centroid structures of olcegepant, ubrogepant, and rimegepant were then superimposed with their corresponding crystal or induced fit structures and showed very few differences in their pose (Figure 3). The piperazinopyridine portion of olcegepant showed slight deviation from the initial crystal pose, represented in the ligand RMSD with an average RMSD of 2.3±0.2 Å. This value is twice larger than those of ubrogepant and rimegepant at 0.8±0.1 Å and 1.0±0.3 Å, respectively. Trajectory clustering analysis reveals a representative conformation for both ubrogepant and rimegepant that show very few differences from the proposed induced fit pose.

MM-GBSA results reveal the order of the ligand binding energy to be olcegepant > ubrogepant > rimegepant. MM-GBSA calculations were performed on each of the MD simulations and revealed that olcegepant is bound most tightly to the receptor, followed by ubrogepant, then rimegepant. The calculated total binding energy for olcegepant is the strongest among the three ligands at -151.9 kcal/mol. Ubrogepant is the next strongest with a total binding energy of -124.3 kcal/mol. Rimegepant follows with a total binding energy of -116.9 kcal/mol (Table S1).

Changes in energy decompositions, with reference to olcegepant, were calculated for ubrogepant and rimegepant (Table S1). Ubrogepant showed a 9.7 kcal/mol decrease in van der

Waals interactions, 13.5 kcal/mol decrease in hydrophobic/lipophilic interactions, and 4.5 kcal/mol decrease in electrostatic interactions. This sums to a 27.6 kcal/mol decrease in total binding energy from olcegepant to ubrogepant, largely due to reduced hydrophobic interactions. Rimegepant showed a 5.5 kcal/mol decrease in van der Waals interactions, 16.2 kcal/mol decrease in hydrophobic/lipophilic interactions, and 12.1 kcal/mol decrease in electrostatic interactions. This sums to a 35.0 kcal/mol decrease in total binding energy from olcegepant to rimegepant, largely due to a decrease in both hydrophobic and electrostatic interactions.

The binding energy data provides encouraging results as they share the same trend as previously reported experimental IC_{50} values, with olcegepant being the strongest binding ligand, and rimegepant, the weakest. Olcegepant has the highest binding affinity with an IC_{50} value of 0.030nM, followed by ubrogepant's 0.80nM, then rimegepant's 0.14 nM [21] [30] [32]. Energy decomposition data show that, from olcegepant to ubrogepant, there is a large decrease in hydrophobic interactions. From olcegepant to rimegepant, the large decrease in binding affinity can be attributed to a decrease in both hydrophobic and electrostatic interactions. It should be kept in mind that olcegepant is a charged +2 molecule and rimegepant is a charged +1 molecule, which may contribute to some of the differences in electrostatic interactions. By comparing ubrogepant and rimegepant binding energy decomposition, ubrogepant's tighter binding can be attributed to an increase in favorable electrostatic interactions with the receptor.

Protein-ligand interaction analysis reveal conserved and novel residue interactions in all three ligands. Olcegepant, ubrogepant, and rimegepant protein-ligand interactions were analyzed using the SID (Figure 4, Figure 5, Figure S7-12). Residues interacting with the ligand more than 0.1 fraction of the simulation time were tabulated and dynamic contacts were recorded (Table S2, Figure S13-15). Previous studies performed on the crystal structure of olcegepant and

its receptor identified three important binding interactions between the receptor and olcegepant, including, but not limited to, the $T122^{ECD}$, $W74^{RAMP1}$, and $W84^{RAMP1}$ residues [40]. These same interactions were reproduced in our molecular dynamics simulation. Furthermore, these three residues were among the six residues conserved across all three ligands: $W72^{ECD}$, $W121^{ECD}$, $T122^{ECD}$, $Y124^{ECD}$, $W74^{RAMP1}$, and $W84^{RAMP1}$. These six conserved residues exhibit either hydrophobic or hydrogen bonding interactions with each of the three ligands.

Of the six conserved residues, $T122^{ECD}$ is one of interest because it makes interactions with the conserved structural feature of all three ligands. In a study by ter Haar et al., researchers established that olcegepant's dihydroquinazolinone structure acts as a hydrogen bond acceptor to the backbone of the $T122^{ECD}$ residue [40]. This residue interaction was reproduced in our MD simulation of olcegepant. Molecular dynamics simulations reveal similar interactions between $T122^{ECD}$ and ubrogepant, as well as $T122^{ECD}$ and rimegepant. This residue exhibits hydrogen bonding with the dihydroquinazolinone portion of olcegepant, the dihydropyrrolopyridinone of ubrogepant, and the dihydroimidazopyridinone of rimegepant. $T122^{ECD}$ has an interaction fraction of 1.808 with olcegepant, 1.971 with ubrogepant, and 1.857 with rimegepant. These conserved interactions suggest that the dihydroquinazolinone derivatives of each antagonist are the pharmacophore of the gepant class.

The $W74^{RAMP1}$ and $W84^{RAMP1}$ residues are also noteworthy because they are residues in the RAMP1 protein that exhibit conserved interactions among all three ligands. As mentioned previously, different RAMPs associated with the CLR can lead to different ligand specificity [4]. Researchers have also reported that the indole of the $W74^{RAMP1}$ sidechain results in stacking of the aliphatic portion of the lysine terminus in olcegepant [40]. $W74^{RAMP1}$ is a key residue for selective binding of the gepant class as seen in experimental binding assays with rats. In one

study, a mutagenesis substitution at this position from lysine (the homologous amino acid in the human receptor) to tryptophan resulted in a 100-fold increase of binding of antagonists. This was attributed to favorable hydrophobic interactions between W74 and the antagonists [44]. The $W74^{RAMP1}$ residue only appears in RAMP1, and not in other CLR/RAMP counterparts such as CLR/RAMP2 or CLR/RAMP3, both of which are adrenomedullin receptors [45]. The CLR/RAMP1 complex's selectivity for antagonists such as olcegepant has been attributed to the presence of the $W74^{RAMP1}$ residue. $W84^{RAMP1}$ of RAMP1 also contributes to this selectivity because it is the residue that forms the hydrophobic pocket in tandem with $W74^{RAMP1}$ [40]. Our study reproduces the interactions between olcegepant and the $W74^{RAMP1}$ and $W84^{RAMP1}$ residues. $W74^{RAMP1}$ has an interaction fraction of 0.911 with olcegepant, 0.421 with ubrogepant, and a doubled 1.915 with rimegepant. While $W74^{RAMP1}$ interacts hydrophobically with all three ligands, it exhibits additional, strong hydrogen bonding with rimegepant's amide carbonyl group, increasing their interaction fraction. $W84^{RAMP1}$ interacts hydrophobically with an interaction fraction of 0.488 with olcegepant, 0.682 with ubrogepant, and 0.351 with rimegepant. Both $W74^{RAMP1}$ and $W84^{RAMP1}$ make up the hydrophobic binding pocket of the receptor and contribute to ligand specificity.

Contact between the antagonists and $W72^{ECD}$ may also be noteworthy as the trend correlates well with the trend of MM-GBSA values. Olcegepant and $W72^{ECD}$ had an interaction fraction of 2.000, consisting of both hydrophobic and hydrogen bonding interactions. Ubrogepant and $W72^{ECD}$ had an interaction fraction of 1.941. Rimegepant and $W72^{ECD}$ had an interaction fraction of 1.798. These values show that between the $W72^{ECD}$ and the antagonist, olcegepant makes the strongest interactions, followed by ubrogepant, then rimegepant. All three drugs exhibit both hydrophobic and hydrogen bonding interactions with $W72^{ECD}$. Researchers have also previously

determined that $W72^{ECD}$ forms a hydrogen bond between the indole of tryptophan and the carbonyl oxygen of olcegepant's amide bond. This creates a "shelf" for the piperidine group of the olcegepant to sit on [36]. In our study, this hydrogen bond between $W72^{ECD}$ and olcegepant's amide bond is reproduced. Similarly, ubrogepant exhibits hydrogen bonding between its amide carbonyl and the indole of $W72^{ECD}$. Dissimilarly, $W72^{ECD}$ did not form a hydrogen bond with the amide carbonyl of rimegepant, but instead formed a hydrogen bond with the nitrogen of the cycloheptenopyridine group.

It can also be noted that there are unique interactions made with the FDA approved ligands, ubrogepant and rimegepant, that were not present with olcegepant: $M42^{ECD}$ and $A70^{RAMP1}$. Both $M42^{ECD}$ and $A70^{RAMP1}$ make hydrophobic contacts with ubrogepant and rimegepant. $M42^{ECD}$ has an interaction fraction of 0.263 with ubrogepant and 0.423 with rimegepant.

Secondary structure examination shows very few differences. The simulation interaction diagram shows the evolution of secondary structure over time. Both alpha helices and beta sheets are shown for the two proteins of the receptor: RAMP1 and the ECD of the CLR (Figure 6, Figure S16-18). The three complexes of olcegepant, ubrogepant, and rimegepant are similar with no notable differences.

Protein and Ligand RMSF show fluctuation in localized regions. The protein $C\alpha$ RMSF plots are used to characterize local changes along the $C\alpha$ protein backbone during simulation (Figure 7, Figure S19-21). PDBSum was used to create topological maps of the secondary structures to locate residues [43]. Peaks of fluctuation in the ECD can be attributed to looped regions of the protein that are typically less stable. Fluctuations in RAMP1 are at the C terminal end of the protein. The moving average RMSF values were also calculated (Table 3). Heavy atoms were

used to calculate ligand RMSF to give novel insight about how the molecule moves (Figure 8, Figure S22-24). Olcegepant shows greatest fluctuation at the aliphatic lysine portion of the molecule with an average of 2.0 Å fluctuation, followed by an averaged 1.5 Å fluctuation of the piperazinopyridine. This is also reflected in trajectory clustering analysis, where the greatest fluctuation of olcegepant occurs at the described regions. Ubrogepant shows greatest fluctuation at its trifluoro group, at an average of 1.2 Å. The rest of the ligand maintains an average of 0.6 Å fluctuation. Rimegepant shows relative stability with all heavy atoms around 0.7 Å RMSF.

Superimposition of crystal structures reveals mode of antagonism. Previous experimental data has suggested that olcegepant acts as a competitive inhibitor of the ECD/RAMP1 receptor [29]. The proposed mechanism is that the antagonist blocks the C-terminal of the CGRP agonist [25]. Interestingly, the superimposition of the full-length cryo-EM structure and crystal structure of olcegepant has shown that the binding positions of olcegepant's dihydroquinazolinone and the CGRP's C-terminal are close to each other, allowing the antagonist to block the binding of the CGRP C-terminal to the transmembrane domain of the CLR/RAMP1 receptor (Figure S1). In addition, the results of our MD simulations show that the binding positions and binding modes of the three compounds olcegepant, ubrogepant, and rimegepant are similar, suggesting that both ubrogepant and rimegepant also antagonize CGRP through competitive inhibition (Figure S25). Thus, all three antagonists could potentially block the C-terminus of the CGRP. By preventing CGRP from binding to the CLR/RAMP1 receptor, the G_s-protein complex will not activate cAMP and cause vasodilation [2, 25].

III. Conclusion

The gepant class of drugs has been found to effectively treat migraines through antagonistic

competitive inhibition of the CGRP receptor. Olcegepant, the predecessor of ubrogepant and rimegepant, was discontinued due to the nature of its delivery being intravenous as opposed to oral. Prior studies have been performed to solve the crystal structure of the receptor and olcegepant, but no crystal structure exists for the FDA approved ubrogepant and rimegepant. This study uses molecular docking and molecular dynamics simulations to propose induced fit poses for both and identify key binding interactions between the receptor and the ligands. From the induced fit ligand pose, results suggest that ubrogepant and rimegepant also antagonize CGRP through competitive inhibition. SID analysis revealed that ubrogepant and rimegepant make critical binding interactions with $T122^{ECD}$, $W74^{RAMP1}$, and $W84^{RAMP1}$ residues that are conserved interactions across all three studied ligands. These three critical interactions reveal the pharmacophore of the gepant class to be the dihydroquinazolinone group derivatives of each ligand. SID analysis also revealed slight differences in interaction profiles, specifically in the interaction with $W74^{RAMP1}$ in which rimegepant has an interaction fraction twice that of olcegepant and ubrogepant. New interactions that appear in the FDA approved drugs are namely hydrophobic interactions between $M42^{ECD}$ and $A70^{RAMP1}$.

MM-GBSA results reveal the binding affinity of olcegepant to be greater than ubrogepant, whose binding affinity is greater than rimegepant. The binding affinity values correlate with the trend of experimental IC_{50} values. Furthermore, by energy decomposition, it appears that the ubrogepant does not bind as strongly as olcegepant due to a decrease in hydrophobic interactions, while rimegepant does not bind as strongly due to a drop in both hydrophobic and electrostatic interactions.

This study may assist in further development of the gepant class for orally available, more potent inhibitors of the CGRP receptor. By looking at the full-length receptor, it can be noted

that there exist other binding pockets that may be targeted to inhibit the receptor (Figure S1). The simulations in this study were run with the ECD as opposed to the full-length receptor, including the transmembrane domain and G proteins, thus, further studies may be needed to interpret the mechanism in which the gepant class inhibits signal transduction.

IV. Methods

The three compounds in this study underwent systematic workflows (Figure 9). Initially, each ligand was docked into the receptor protein structure with XP precision. This docking uses a rigid receptor and is done as a preliminary step before induced fit docking. Once docked, the ligand-receptor complexes underwent induced fit docking to find the most probable conformational pose. Induced fit docking allows the protein receptor to undergo conformational changes to fit the ligand [54]. The solved crystal structure of olcegepant was used in lieu of an induced fit pose. The induced fit poses or crystal structure of each ligand-receptor complex were then subject to three 1000ns molecular dynamics simulations. Analysis of the simulation interaction diagrams was performed, followed by structural clustering and MM-GBSA calculations.

1. Preparation of Ligands

Olcegepant's 3D structure was taken from the crystal ligand-receptor complex, downloaded from the RCSB Protein Data Bank [46]. The 2D structures for ubrogepant and rimegepant were downloaded from the ZINC15 database [47], corrected for bond orders, and converted to 3D models in Maestro. Ionization states were generated at a pH of 7 using Epik's pKa calculations [48] [49]. Ligands were then relaxed by minimization with Maestro's Protein Preparation Wizard tool and procedures, using the OPLS3e forcefield. The OPLS3e forcefield utilizes a

parametrization approach to systematically assign charges [49] [50]. The 2D structures of each ligand were also submitted to the SwissADME database to calculate solubility based on the ESOL method [41] [42].

2. Preparation of CGRP Receptor

Previous studies of the gepants class show olcegepant and telcagepant interacting mainly at the ECD and RAMP1 interface [40]. As a result, the transmembrane domain and G proteins of the CGRP receptor were omitted in this study to reduce computational costs. A crystal structure of the remaining ECD/RAMP1 complex was taken from the RCSB Protein Data Bank (PDB ID: 3N7R) [40]. This crystal structure included the crystal ligand, olcegepant, and the truncated CGRP receptor. The ligand was removed to reveal only the ECD/RAMP1 complex that was then subjected to homology modeling to repair a missing loop in the ECD structure (Figure S26). The homology modelled ECD/RAMP1 structure was then minimized to relax the protein using Maestro's Protein Preparation Wizard in an OPLS3e force field with default parameters [49] [50] [51].

3. Ligand docking

The fully prepared ECD/RAMP1-olcegepant crystal complex was used to define the binding site of the receptor. In order to validate Schrodinger Maestro's Extra Precision (XP) Glide Docking methods [52] [53], the prepared olcegepant ligand was docked into the ECD/RAMP1 receptor complex (XP docking score: -12.77 kcal/mol). Its docking pose was then compared to the crystal structure. The ligand RMSD between the crystal structure and docked olcegepant was 0.943 Å, indicating little deviation and validating our docking protocol (Figure S27). Ubrogepant (XP docking score: -10.15 kcal/mol) and rimegepant (XP docking score: -9.69 kcal/mol) were subsequently docked into the ECD/RAMP1 receptor and their poses were compared to that of

olcegepant (Figure S28). Once all ligands have undergone Glide XP docking, ubrogepant and rimegepant underwent induced fit docking under default parameters to generate multiple poses of ligand complex that include structural modifications of the receptor (Figure S29) [54]. The induced fit docking poses generated were manually evaluated based on binding score and similarity to the crystal ligand olcegepant's binding pose. Finally, the selected induced fit poses for ubrogepant and rimegepant, as well as the crystal structure of olcegepant, were used for molecular dynamics simulation (Figure 10).

4. Preparation of Molecular Dynamics Simulation

Three separate systems were prepared for a 1000 ns molecular dynamics simulation. Each system included the ECD/RAMP1 protein structure in complex with a ligand: olcegepant, ubrogepant, or rimegepant. These three systems were solvated in a simple point-charge (SPC) orthorhombic water box with a 10 Å water buffer between the complex and the water box boundary [55]. The olcegepant system consisted of 7631 waters, ubrogepant of 9841 waters, and rimegepant of 7649 waters. They were then neutralized by counter ions and 0.15 M NaCl was added. Each system was built with an OPLS3e force field using the Desmond System Builder with Maestro's 2019-2 update [50].

The molecular dynamics (MD) simulations were performed with Schrodinger Maestro's Desmond simulation package [56] [57]. The three systems were relaxed using the default protocol and energy minimizations were performed to reduce possible steric stress [58]. First, the systems were minimized with restraints on solute heavy atoms and then once more without restraints. Next, the systems were simulated in an NVT ensemble with a heat transition from 0 to 300K, in a water barrier, and with restraining on solute heavy atoms. Then, the systems were simulated in an NPT (P = 1 bar, T = 310K) ensemble with a water barrier and solute heavy atom

restraints. The systems were simulated in the NPT ensemble with an equilibrium of both solvent and solute. Then, systems were simulated under NPT ensemble with protein heavy atoms annealing from 10.0 to 2.0 kcal/mol. Systems were then simulated under NPT ensemble with $C\alpha$ atoms restrained at 2 kcal/mol. Finally, they were simulated for 1.5 ns under the NPT ensemble with no restraints. After relaxation, the three systems were run for 1000 ns using NPT ensemble (P = 1 bar and T = 310 K). In these simulations, temperature was controlled by the Nosé-Hoover chain coupling scheme with a coupling constant of 1.0 ps [59], and pressure was controlled by the Martyna-Tuckerman-Klein chain coupling scheme with a coupling constant of 2.0 ps [59]. All bonds connected to hydrogen atoms were constrained by applying M-SHAKE [60] and enabling a 2.0 fs time-step within the simulations. Long-range electrostatic interactions were analyzed using the k-space Gaussian split Ewald method [61] under periodic boundary conditions, with a charge grid spacing of ~ 1.0Å and a direct sum tolerance of 10^{-9}. The short-range non-bonded interactions had a cutoff distance of 10Å. The long-range van der Waals interactions were based on a uniform density approximation. To condense the computation, an r-RESPA integrator was used to calculate non-bonded forces [62], where every step the short-range forces were updated and every three steps the long-range forces were updated. Three trajectories were run for each system and saved at 50.0 ps intervals for analysis.

5. Simulation Interaction Diagram (SID) Analysis

The Desmond simulation interaction diagram (SID) analysis tool depicts the interactions between the receptor and ligand during molecular dynamics simulation. This analysis report includes protein-ligand root mean squared deviation (RMSD), protein-ligand contacts, protein root-mean squared fluctuation (RMSF), changes in secondary structure elements (SSE) during

the simulation, and ligand torsion profiles. The protein and ligand RMSD plots were analyzed to ensure the convergence of the MD simulations.

6. Trajectory clustering Analysis

The Desmond trajectory clustering analysis tool [63] uses the structures from the MD simulation to group complex structure. The backbone RMSD matrix is used as the basis of structural similarity and the clustering with average linkage was cut off at 2.5 Å [63]. The centroid structure of the protein-ligand complex was used to represent each structural family. Structural families with frames >1% of the total frames were considered separate structural families with separate centroid structures.

7. Binding Energy Calculations and decompositions methods

Molecular Mechanism - Generalized Born Surface Area (MM-GBSA) binding energies were calculated using snapshots of the last 200 ns of the simulation. Previous studies assessing the validity of MM-GBSA have been performed [64-69]. The calculations used an OPLS3e force field**,** a VSGB 2.0 solvation model and the default Prime protocol [51]. First, the receptor was minimized, followed by the ligand, and finally the receptor-ligand complex. The total binding energy equation is as follows: $\Delta G_{bind} = G_{complex} - (G_{ligand} + G_{receptor})$. The binding energy was broken down into three components: $G_{electrostatic,}$ $G_{vdW,}$ and $G_{lipophilic}$. $G_{electrostatic}$ was calculated by summing $G_{H\text{-}bond}$ and $G_{coulumbic}$. G_{vdW} summated G_{vdW}, $G_{pi\text{-}pi\ stacking}$, and $G_{self\text{-}contact}$. ΔG_{bind} is the total Gibbs free binding energy in kcal/mol (Table S1)**.** It should be noted that entropy was omitted from the Gibbs free binding energy calculation. While this may lead to an overestimation for MM-GBSA, the compounds are assumed to have similar entropic contributions due to their similar structure, and entropic contribution has been omitted.

Author Contribution

Conceptualization, C.W.; Formal Analysis, L.L. and S.L.; Writing – Original Draft Preparation, L.L. and S. L.; Writing – Review & Editing, C.W.

Acknowledgements:

We acknowledge the support by New Jersey Health Foundation (PC 76-21) and the National Science Foundation under Grants NSF ACI-1429467/RUI-1904797, and XSEDE MCB 170088. The Anton2 machine at the Pittsburgh Supercomputing Center (PSCA17017P) was generously made available by D. E. Shaw Research.

Supporting Information

Includes detailed structural information and simulation interaction diagram analysis on individual trajectories of each system. Homology modelling, docking results, MM-GBSA binding energy breakdown, and 3D interaction diagrams are also included. Movies of ubrogepant, rimegepant, and olcegepant trajectory system are also accessible. Mol2 files of each ligand are also available: olcegepant.mol2, ubrogepant.mol2, rimegepant.mol2 to show spatial location and partial charge of each atom.

References

1. Collaborators, G.B.D.H., *Global, regional, and national burden of migraine and tension-type headache, 1990-2016: a systematic analysis for the Global Burden of Disease Study 2016.* Lancet Neurol, 2018. **17**(11): p. 954-976.
2. Goadsby, P.J., L. Edvinsson, and R. Ekman, *Vasoactive peptide release in the extracerebral circulation of humans during migraine headache.* Annals of Neurology, 1990. **28**(2): p. 183-187.
3. Hollenstein, K., J. Kean, A. Bortolato, R.K. Cheng, A.S. Dore, A. Jazayeri, R.M. Cooke, M. Weir, and F.H. Marshall, *Structure of class B GPCR corticotropin-releasing factor receptor 1.* Nature, 2013. **499**(7459): p. 438-43.
4. Bortolato, A., A.S. Doré, K. Hollenstein, B.G. Tehan, J.S. Mason, and F.H. Marshall, *Structure of C lass B GPCRs : new horizons for drug discovery*. 2014. p. 3132-3145.
5. Liang, Y.L., M. Khoshouei, M. Radjainia, Y. Zhang, A. Glukhova, J. Tarrasch, D.M. Thal, S.G.B. Furness, G. Christopoulos, T. Coudrat*, et al.*, *Phase-plate cryo-EM structure of a class B GPCR-G-protein complex.* Nature, 2017. **546**(7656): p. 118-123.
6. Siu, F.Y., M. He, C. de Graaf, G.W. Han, D. Yang, Z. Zhang, C. Zhou, Q. Xu, D. Wacker, J.S. Joseph*, et al.*, *Structure of the human glucagon class B G-protein-coupled receptor.* Nature, 2013. **499**(7459): p. 444-9.
7. Harmar, A.J., *Family-B G-protein-coupled receptors.* Genome Biol, 2001. **2**(12): p. REVIEWS3013.
8. Barwell, J., D. Wootten, J. Simms, D.L. Hay, and D.R. Poyner, *RAMPs and CGRP receptors.* Adv Exp Med Biol, 2012. **744**: p. 13-24.
9. Booe, J.M., C.S. Walker, J. Barwell, G. Kuteyi, J. Simms, M.A. Jamaluddin, M.L. Warner, R.M. Bill, P.W. Harris, M.A. Brimble*, et al.*, *Structural Basis for Receptor Activity-Modifying Protein-Dependent Selective Peptide Recognition by a G Protein-Coupled Receptor.* Mol Cell, 2015. **58**(6): p. 1040-52.
10. Booe, J.M., M.L. Warner, A.M. Roehrkasse, D.L. Hay, and A.A. Pioszak, *Probing the Mechanism of Receptor Activity-Modifying Protein Modulation of GPCR Ligand Selectivity through Rational Design of Potent Adrenomedullin and Calcitonin Gene-Related Peptide Antagonists.* Mol Pharmacol, 2018. **93**(4): p. 355-367.
11. Choksi, T., D.L. Hay, S. Legon, D.R. Poyner, S. Hagner, S.R. Bloom, and D.M. Smith, *Comparison of the expression of calcitonin receptor-like receptor (CRLR) and receptor activity modifying proteins (RAMPs) with CGRP and adrenomedullin binding in cell lines.* Br J Pharmacol, 2002. **136**(5): p. 784-92.
12. Conner, A.C., J. Simms, D.L. Hay, K. Mahmoud, S.G. Howitt, M. Wheatley, and D.R. Poyner, *Heterodimers and family-B GPCRs: RAMPs, CGRP and adrenomedullin.* Biochem Soc Trans, 2004. **32**(Pt 5): p. 843-6.
13. Gingell, J.J., E.R. Hendrikse, and D.L. Hay, *New Insights into the Regulation of CGRP-Family Receptors.* Trends Pharmacol Sci, 2019. **40**(1): p. 71-83.
14. Hay, D.L. and A.A. Pioszak, *Receptor Activity-Modifying Proteins (RAMPs): New Insights and Roles.* Annu Rev Pharmacol Toxicol, 2016. **56**: p. 469-87.
15. J, J.G., J. Simms, J. Barwell, D.R. Poyner, H.A. Watkins, A.A. Pioszak, P.M. Sexton, and D.L. Hay, *An allosteric role for receptor activity-modifying proteins in defining GPCR pharmacology.* Cell Discov, 2016. **2**: p. 16012.

16. Simms, J., S. Routledge, R. Uddin, and D. Poyner, *The Structure of the CGRP and Related Receptors*, in *Calcitonin Gene-Related Peptide (CGRP) Mechanisms: Focus on Migraine*, S.D. Brain and P. Geppetti, Editors. 2019, Springer International Publishing: Cham. p. 23-36.
17. Watkins, H.A., M. Chakravarthy, R.S. Abhayawardana, J.J. Gingell, M. Garelja, M. Pardamwar, J.M. McElhinney, A. Lathbridge, A. Constantine, P.W. Harris*, et al.*, *Receptor Activity-modifying Proteins 2 and 3 Generate Adrenomedullin Receptor Subtypes with Distinct Molecular Properties.* J Biol Chem, 2016. **291**(22): p. 11657-75.
18. Bohn, K.J., B. Li, X. Huang, B.N. Mason, A.S. Wattiez, A. Kuburas, C.S. Walker, P. Yang, J. Yu, B.A. Heinz*, et al.*, *CGRP receptor activity in mice with global expression of human receptor activity modifying protein 1.* Br J Pharmacol, 2017. **174**(12): p. 1826-1840.
19. Bailey, R.J., C.S. Walker, A.H. Ferner, K.M. Loomes, G. Prijic, A. Halim, L. Whiting, A.R. Phillips, and D.L. Hay, *Pharmacological characterization of rat amylin receptors: implications for the identification of amylin receptor subtypes.* Br J Pharmacol, 2012. **166**(1): p. 151-67.
20. Woolley, M.J., C.A. Reynolds, J. Simms, C.S. Walker, J.C. Mobarec, M.L. Garelja, A.C. Conner, D.R. Poyner, and D.L. Hay, *Receptor activity-modifying protein dependent and independent activation mechanisms in the coupling of calcitonin gene-related peptide and adrenomedullin receptors to Gs.* Biochem Pharmacol, 2017. **142**: p. 96-110.
21. Dubowchik, G.M., C.M. Conway, and A.W. Xin, *Blocking the CGRP Pathway for Acute and Preventive Treatment of Migraine: The Evolution of Success.* Journal of medicinal chemistry, 2020. **63**(13): p. 6600.
22. Hay, D.L., A.C. Conner, S.G. Howitt, D.M. Smith, and D.R. Poyner, *The pharmacology of adrenomedullin receptors and their relationship to CGRP receptors.* J Mol Neurosci, 2004. **22**(1-2): p. 105-13.
23. Hay, D.L., M.L. Garelja, D.R. Poyner, and C.S. Walker, *Update on the pharmacology of calcitonin/CGRP family of peptides: IUPHAR Review 25.* Br J Pharmacol, 2018. **175**(1): p. 3-17.
24. Liang, Y.L., M. Khoshouei, G. Deganutti, A. Glukhova, C. Koole, T.S. Peat, M. Radjainia, J.M. Plitzko, W. Baumeister, L.J. Miller*, et al.*, *Cryo-EM structure of the active, Gs-protein complexed, human CGRP receptor.* Nature, 2018. **561**(7724): p. 492-497.
25. Chiba, T., A. Yamaguchi, T. Yamatani, A. Nakamura, T. Morishita, T. Inui, M. Fukase, T. Noda, and T. Fujita, *Calcitonin gene-related peptide receptor antagonist human CGRP-(8-37).* Am J Physiol, 1989. **256**(2 Pt 1): p. E331-5.
26. Ho, T.W., K.M. Connor, Y. Zhang, E. Pearlman, J. Koppenhaver, X. Fan, C. Lines, L. Edvinsson, P.J. Goadsby, and D. Michelson, *Randomized controlled trial of the CGRP receptor antagonist telcagepant for migraine prevention.* Neurology, 2014. **83**(11): p. 958-66.
27. Ho, T.W., A.P. Ho, Y.J. Ge, C. Assaid, R. Gottwald, E.A. MacGregor, L.K. Mannix, W.P. van Oosterhout, J. Koppenhaver, C. Lines*, et al.*, *Randomized controlled trial of the CGRP receptor antagonist telcagepant for prevention of headache in women with perimenstrual migraine.* Cephalalgia, 2016. **36**(2): p. 148-61.

28. Yao, G., T. Yu, X. Han, X. Mao, and B. Li, *Therapeutic effects and safety of olcegepant and telcagepant for migraine: A meta-analysis.* Neural Regen Res, 2013. **8**(10): p. 938-47.
29. Doods, H., G. Hallermayer, D. Wu, M. Entzeroth, K. Rudolf, W. Engel, and W. Eberlein, *Pharmacological profile of BIBN4096BS, the first selective small molecule CGRP antagonist.* Br J Pharmacol, 2000. **129**(3): p. 420-3.
30. Scott, L.J., *Ubrogepant: First Approval.* Drugs, 2020. **80**(3): p. 323.
31. Dodick, D.W., R.B. Lipton, J. Ailani, K. Lu, M. Finnegan, J.M. Trugman, and A. Szegedi, *Ubrogepant for the Treatment of Migraine.* The New England journal of medicine, 2019. **381**(23): p. 2230.
32. Scott, L.J., *Rimegepant: First Approval.* Drugs, 2020. **80**(7): p. 741.
33. Lipton, R.B., R. Croop, E.G. Stock, D.A. Stock, B.A. Morris, M. Frost, G.M. Dubowchik, C.M. Conway, V. Coric, and P.J. Goadsby, *Rimegepant, an Oral Calcitonin Gene-Related Peptide Receptor Antagonist, for Migraine.* The New England journal of medicine, 2019. **381**(2): p. 142.
34. Johnston, K., E. Popoff, A. Deighton, P. Dabirvaziri, L. Harris, A. Thiry, R. Croop, V. Coric, and G. L'Italien, *Comparative Efficacy and Safety of Rimegepant Versus Ubrogepant and Lasmiditan for Acute Treatment of Migraine: A Network Meta-analysis (NMA)(4369)*. 2020, AAN Enterprises.
35. Blumenfeld, A.M., L. Edvinsson, A. Jakate, and P. Banerjee, *Pharmacology and Pharmacokinetics of Ubrogepant: A Potent, Selective Calcitonin Gene-Related Peptide Receptor Antagonist for the Acute Treatment of Migraine.* Journal of Family Practice, 2020. **69**(1): p. S8.
36. Moore, E., M.E. Fraley, I.M. Bell, C.S. Burgey, R.B. White, C.C. Li, C.P. Regan, A. Danziger, M. Stranieri Michener, E. Hostetler*, et al.*, *Characterization of Ubrogepant: A Potent and Selective Antagonist of the Human Calcitonin GeneRelated Peptide Receptor.* J Pharmacol Exp Ther, 2020.
37. Kylie, S.P., S. Andrew, L.H. Debbie, and S.W. Christopher, *Antagonism of CGRP Signaling by Rimegepant at Two Receptors.* Frontiers in pharmacology, 2020. **11**.
38. Walker, C.S., A.C. Raddant, M.J. Woolley, A.F. Russo, and D.L. Hay, *CGRP receptor antagonist activity of olcegepant depends on the signalling pathway measured.* Cephalalgia, 2018. **38**(3): p. 437-451.
39. Watkins, H.A., C.S. Walker, K.N. Ly, R.J. Bailey, J. Barwell, D.R. Poyner, and D.L. Hay, *Receptor activity-modifying protein-dependent effects of mutations in the calcitonin receptor-like receptor: implications for adrenomedullin and calcitonin gene-related peptide pharmacology.* Br J Pharmacol, 2014. **171**(3): p. 772-88.
40. Ter Haar, E., C.M. Koth, N. Abdul-Manan, L. Swenson, J.T. Coll, J.A. Lippke, C.A. Lepre, M. Garcia-Guzman, and J.M. Moore, *Crystal Structure of the Ectodomain Complex of the CGRP Receptor, a Class-B GPCR, Reveals the Site of Drug Antagonism.* Structure (London), 2010. **18**(9): p. 1083-1093.
41. Daina, A., O. Michielin, and V. Zoete, *SwissADME: a free web tool to evaluate pharmacokinetics, drug-likeness and medicinal chemistry friendliness of small molecules.* Sci Rep, 2017. **7**: p. 42717.
42. Delaney, J.S., *ESOL: estimating aqueous solubility directly from molecular structure.* J Chem Inf Comput Sci, 2004. **44**(3): p. 1000-5.

43. Laskowski, R.A., J. Jablonska, L. Pravda, R.S. Varekova, and J.M. Thornton, *PDBsum: Structural summaries of PDB entries.* Protein Sci, 2018. **27**(1): p. 129-134.
44. Mallee, J.J., C.A. Salvatore, B. LeBourdelles, K.R. Oliver, J. Longmore, K.S. Koblan, and S.A. Kane, *Receptor activity-modifying protein 1 determines the species selectivity of non-peptide CGRP receptor antagonists.* J Biol Chem, 2002. **277**(16): p. 14294-8.
45. Hay, D.L. and C.S. Walker, *CGRP and its receptors.* Headache, 2017. **57**(4): p. 625-636.
46. Berman, H.M., J. Westbrook, Z. Feng, G. Gilliland, T.N. Bhat, H. Weissig, I.N. Shindyalov, and P.E. Bourne, *The Protein Data Bank.* Nucleic Acids Res, 2000. **28**(1): p. 235-42.
47. Sterling, T. and J.J. Irwin, *ZINC 15--Ligand Discovery for Everyone.* Journal of chemical information and modeling, 2015. **55**(11): p. 2324.
48. Shelley, J.C., A. Cholleti, L.L. Frye, J.R. Greenwood, M.R. Timlin, and M. Uchimaya, *Epik: a software program for pK(a) prediction and protonation state generation for drug-like molecules.* J Comput Aided Mol Des, 2007. **21**(12): p. 681-91.
49. Sastry, G.M., M. Adzhigirey, T. Day, R. Annabhimoju, and W. Sherman, *Protein and ligand preparation: parameters, protocols, and influence on virtual screening enrichments.* J Comput Aided Mol Des, 2013. **27**(3): p. 221-34.
50. Roos, K., C. Wu, W. Damm, M. Reboul, J.M. Stevenson, C. Lu, M.K. Dahlgren, S. Mondal, W. Chen, L. Wang*, et al.*, *OPLS3e: Extending Force Field Coverage for Drug-Like Small Molecules.* J Chem Theory Comput, 2019. **15**(3): p. 1863-1874.
51. Harder, E., W. Damm, J. Maple, C. Wu, M. Reboul, J.Y. Xiang, L. Wang, D. Lupyan, M.K. Dahlgren, J.L. Knight*, et al.*, *OPLS3: A Force Field Providing Broad Coverage of Drug-like Small Molecules and Proteins.* J Chem Theory Comput, 2016. **12**(1): p. 281-96.
52. Friesner, R.A., J.L. Banks, R.B. Murphy, T.A. Halgren, J.J. Klicic, D.T. Mainz, M.P. Repasky, E.H. Knoll, M. Shelley, J.K. Perry*, et al.*, *Glide: A New Approach for Rapid, Accurate Docking and Scoring. 1. Method and Assessment of Docking Accuracy.* J. Med. Chem., 2004. **47**(7): p. 1739-1749.
53. Friesner, R.A., R.B. Murphy, M.P. Repasky, L.L. Frye, J.R. Greenwood, T.A. Halgren, P.C. Sanschagrin, and D.T. Mainz, *Extra Precision Glide: Docking and Scoring Incorporating a Model of Hydrophobic Enclosure for Protein−Ligand Complexes.* J. Med. Chem., 2006. **49**(21): p. 6177-6196.
54. Sherman, W., T. Day, M.P. Jacobson, R.A. Friesner, and R. Farid, *Novel procedure for modeling ligand/receptor induced fit effects.* J Med Chem, 2006. **49**(2): p. 534-53.
55. Mark, P. and L. Nilsson, *Structure and dynamics of liquid water with different long-range interaction truncation and temperature control methods in molecular dynamics simulations.* J Comput Chem, 2002. **23**(13): p. 1211-9.
56. Jorgensen, W.L., D.S. Maxwell, and J. Tirado-Rives, *Development and Testing of the OPLS All-Atom Force Field on Conformational Energetics and Properties of Organic Liquids.* J. Am. Chem. Soc., 1996. **118**(45): p. 11225-11236.
57. Shivakumar, D., J. Williams, Y. Wu, W. Damm, J. Shelley, and W. Sherman, *Prediction of Absolute Solvation Free Energies using Molecular Dynamics Free Energy Perturbation and the OPLS Force Field.* Journal of chemical theory and computation, 2010. **6**(5): p. 1509.

58. Jiapu Zhang, Y.H., Yiju Wang, Changyu Wang, Xiangsun Zhang, *The LBFGS quasi-Newtonian method for molecular modeling prion AGAAAAGA amyloid fibrils.* Natural Science, 2012.
59. Ikeguchi, M., *Partial rigid-body dynamics in NPT, NPAT and NPgammaT ensembles for proteins and membranes.* J Comput Chem, 2004. **25**(4): p. 529-41.
60. Bailey, A.G. and C.P. Lowe, *MILCH SHAKE: an efficient method for constraint dynamics applied to alkanes.* J Comput Chem, 2009. **30**(15): p. 2485-93.
61. Shan, Y., J.L. Klepeis, M.P. Eastwood, R.O. Dror, and D.E. Shaw, *Gaussian split Ewald: A fast Ewald mesh method for molecular simulation.* J Chem Phys, 2005. **122**(5): p. 54101.
62. Morrone, J.A., R. Zhou, and B.J. Berne, *Molecular Dynamics with Multiple Time Scales: How to Avoid Pitfalls.* J Chem Theory Comput, 2010. **6**(6): p. 1798-804.
63. E.C. Bowers, O.R.D., P. Michael Eastwood, A. Brent Gregersen, L. John Klepeis, Istvan Kolossvary, A. Mark Moraes, D. Federico Sacerdoti, K. John, Salmon, Y. Shan, E. David Shaw, *Scalable Algorithms for Molecular Dynamics Simulations on Commodity Clusters.* 2006.
64. Hou, T., J. Wang, Y. Li, and W. Wang, *Assessing the performance of the MM/PBSA and MM/GBSA methods. 1. The accuracy of binding free energy calculations based on molecular dynamics simulations.* J Chem Inf Model, 2011. **51**(1): p. 69-82.
65. Kollman, P.A., I. Massova, C. Reyes, B. Kuhn, S. Huo, L. Chong, M. Lee, T. Lee, Y. Duan, W. Wang*, et al.*, *Calculating structures and free energies of complex molecules: combining molecular mechanics and continuum models.* Acc Chem Res, 2000. **33**(12): p. 889-97.
66. Hou, T., J. Wang, Y. Li, and W. Wang, *Assessing the performance of the molecular mechanics/Poisson Boltzmann surface area and molecular mechanics/generalized Born surface area methods. II. The accuracy of ranking poses generated from docking.* J Comput Chem, 2011. **32**(5): p. 866-77.
67. Sun, H., Y. Li, S. Tian, L. Xu, and T. Hou, *Assessing the performance of MM/PBSA and MM/GBSA methods. 4. Accuracies of MM/PBSA and MM/GBSA methodologies evaluated by various simulation protocols using PDBbind data set.* Phys Chem Chem Phys, 2014. **16**(31): p. 16719-29.
68. Xu, L., H. Sun, Y. Li, J. Wang, and T. Hou, *Assessing the performance of MM/PBSA and MM/GBSA methods. 3. The impact of force fields and ligand charge models.* J Phys Chem B, 2013. **117**(28): p. 8408-21.
69. Kongsted, J., P. Soderhjelm, and U. Ryde, *How accurate are continuum solvation models for drug-like molecules?* J Comput Aided Mol Des, 2009. **23**(7): p. 395-409.

Table 1. Gepant class antagonists

Ligand	Commercial product name	Stage of development	Administration	Crystal Structure with Receptor
Olcegepant	-	Discontinued	intravenous	solved
Telcagepant	-	Discontinued	intravenous	-
Ubrogepant	UBRELVY™	FDA approved December 23, 2019	oral	-
Rimegepant	Nurtec™ ODT	FDA approved February 27, 2020	oral	-

Status of gepant class antagonists.

Table 2. Properties of studied CGRPR antagonists

Ligand	IC_{50} (nM)	MW (Da)	Net Charge	Glide XP Score (kcal/mol)	Water solubility Log S (ESOL)[1]	ΔG (kcal/mol)
Olcegepant	0.030	871.7	+2	-12.8	-6.40	-151.9 ± 2.2
Ubrogepant	0.080	549.6	0	-10.2	-5.14	-124.3 ± 4.6
Rimegepant	0.14	535.6	+1	-9.7	-4.67	-116.9 ± 7.3

[1]Predicted values from SwissADME database.

Table 3. Mean RMSF of receptor complex

	RAMP1 Mean RMSF	ECD Mean RMSF
Olcegepant	0.85 ± 0.31	1.52 ± 1.46
Ubrogepant	1.21 ± 0.49	1.50 ± 1.01
Rimegepant	0.88 ± 0.36	1.17 ± 0.78

RMSF values measured using Cα backbone and first snapshot as reference.

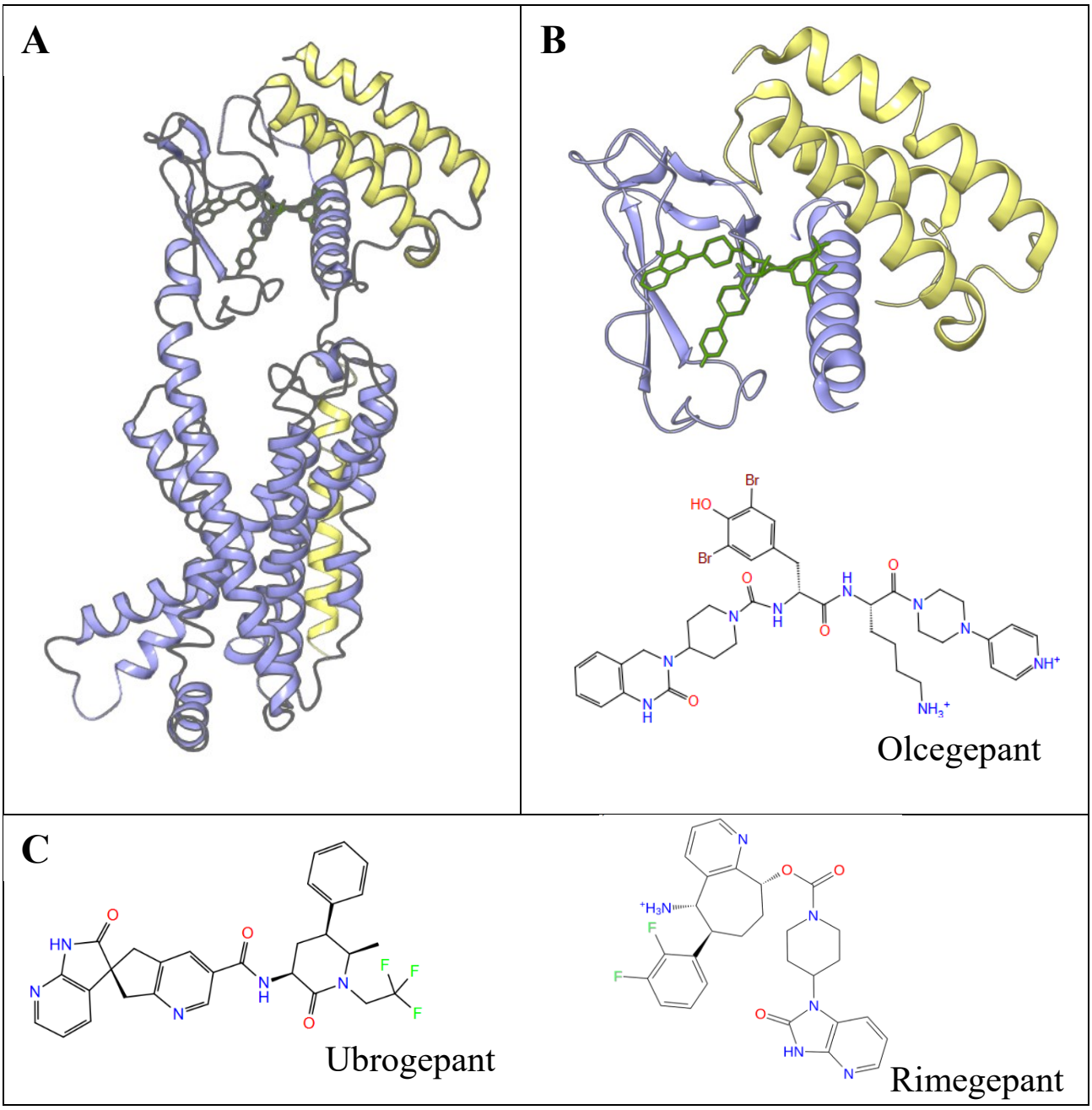

Figure 1. Three studied compounds with their target receptor. Olcegepant binds to the ECD/RAMP1 pocket interface of the CGRPR, and this truncated complex was used as the receptor in this study. **A**: Crystal ligand, olcegepant, docked in full length CGRPR (purple) in complex with receptor activity modifying protein 1 (yellow) [*PDB ID: 6E3Y*]. **B:** Truncated crystal structure of ECD (purple) and RAMP1 (yellow) with crystal ligand olcegepant (green) bound at the pocket interface *[PDB ID: 3N7R*]. Chemical structure of olcegepant displayed below. **C:** Chemical structure of ubrogepant and rimegepant.

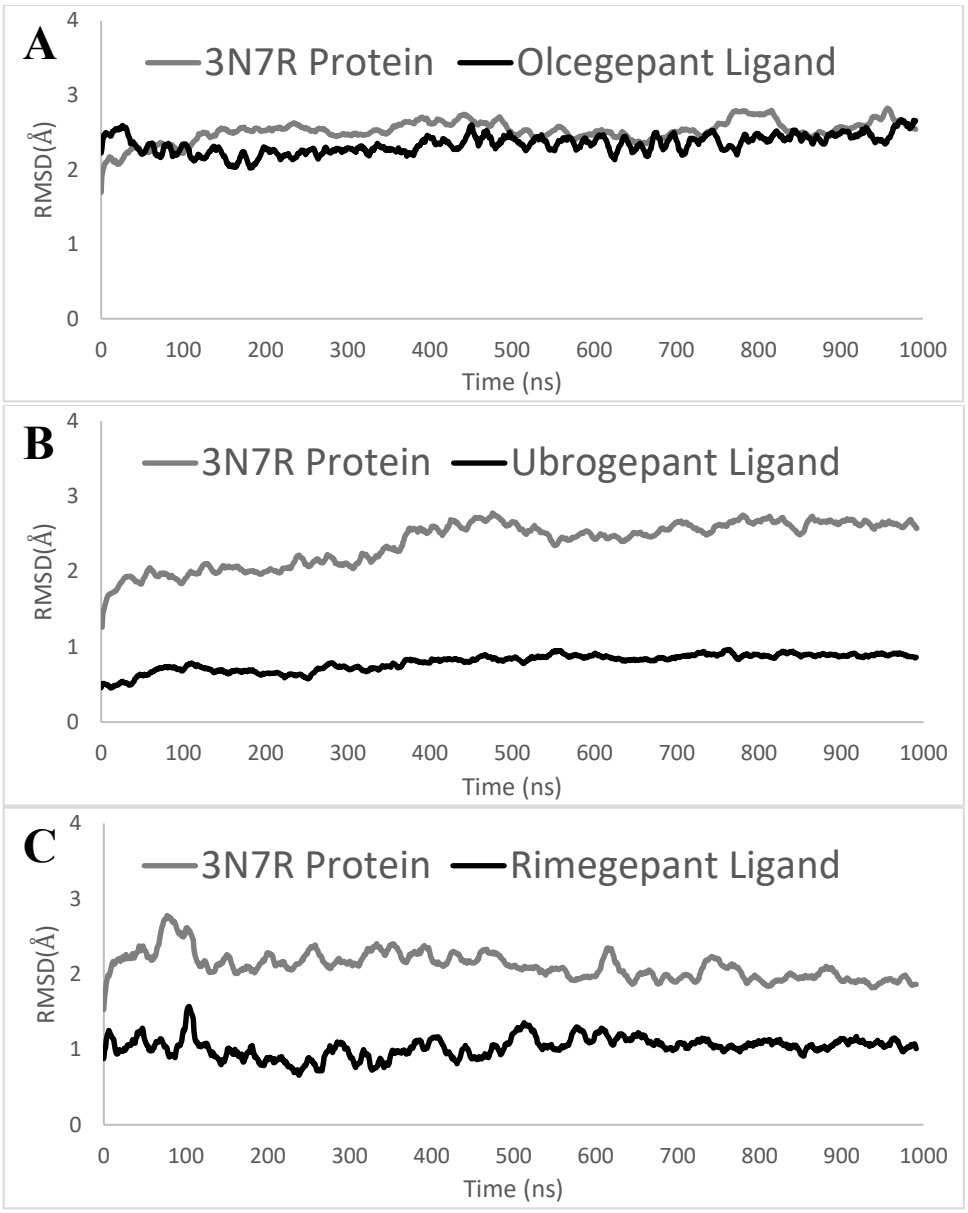

Figure 2. Cα average RMSD of ECD/RAMP1 proteins and three ligands during the three 1000 ns MD simulation trajectories. First snapshot of simulation is used as the reference. **A:** olcegepant **B:** ubrogepant **C:** rimegepant.

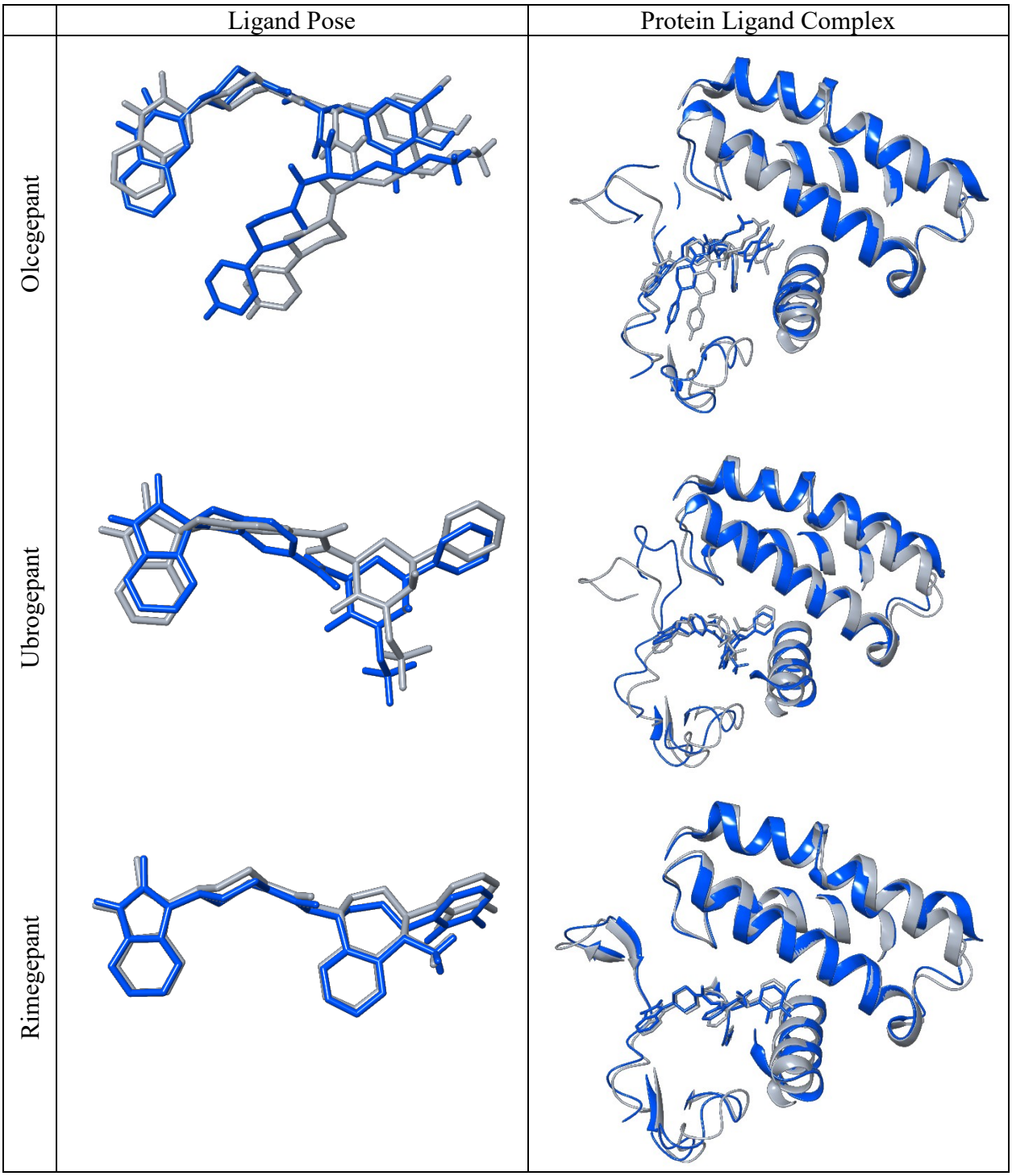

Figure 3. Comparison of centroid structures (blue) from MD simulations with corresponding initial pose (gray). Initial pose for olcegepant is crystal pose, initial poses for ubrogepant and rimegepant are induced fit poses.

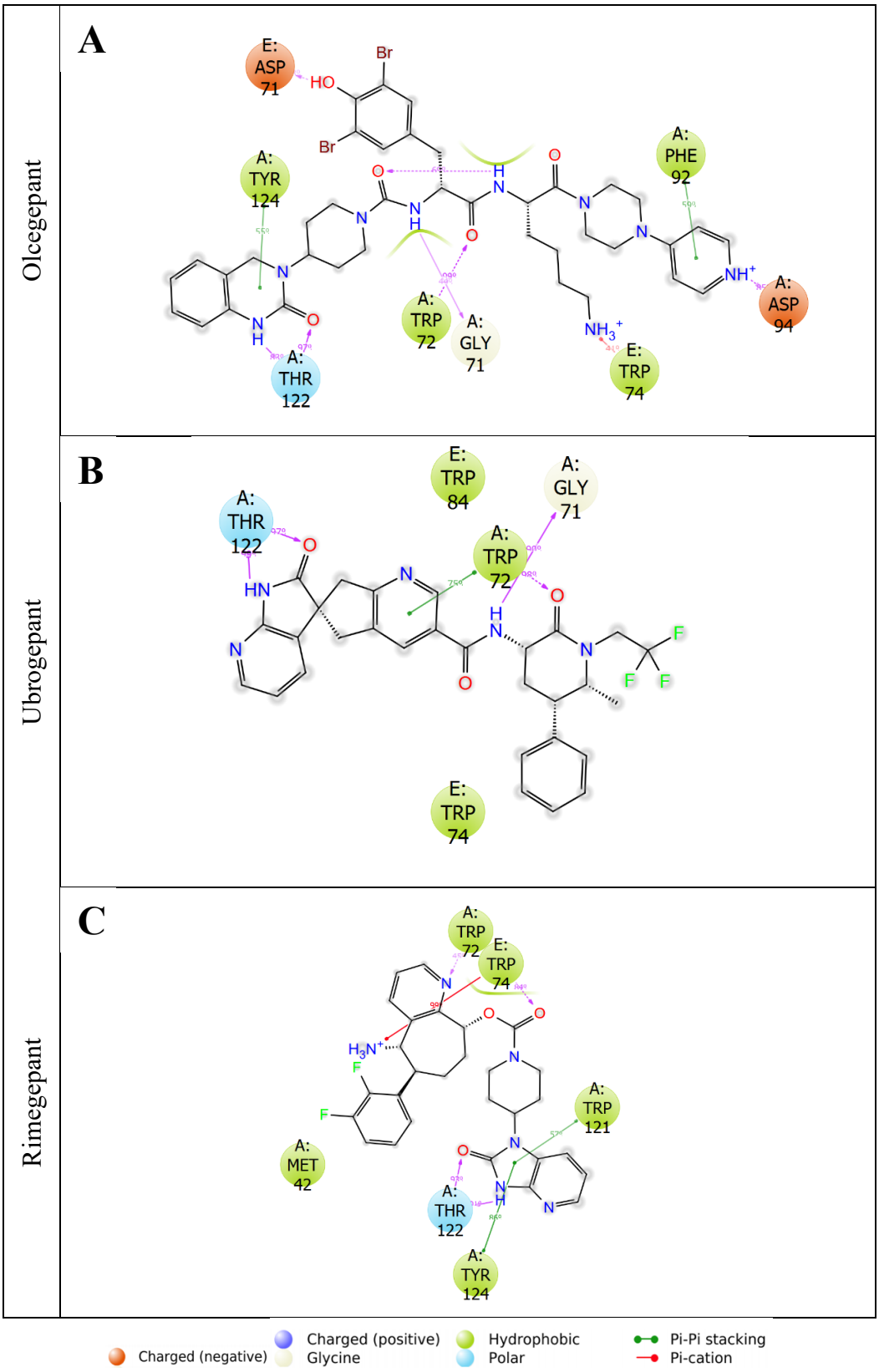

Figure 4. 2D ligand interaction diagrams of trajectory during MD simulation. Residues displayed interacted with ligand for at least 30% of the simulation time.

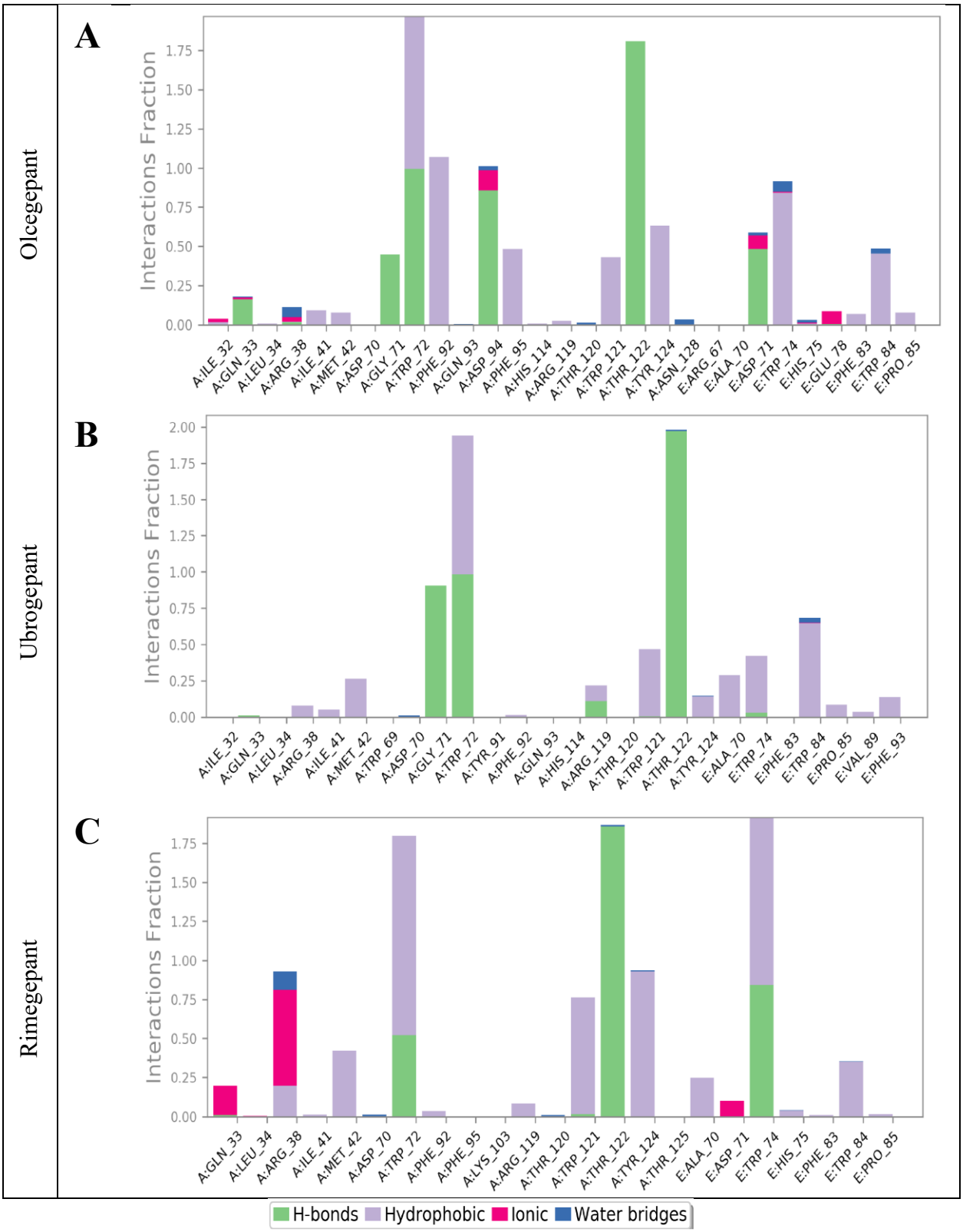

Figure 5. Protein-Ligand contacts during MD simulations. Interaction fraction greater than 1 is possible because of multiple contacts on one residue. Contacts are tabulated in supporting table 2. Residues preceded with "A" belong to ECD and "E" belong to RAMP1.

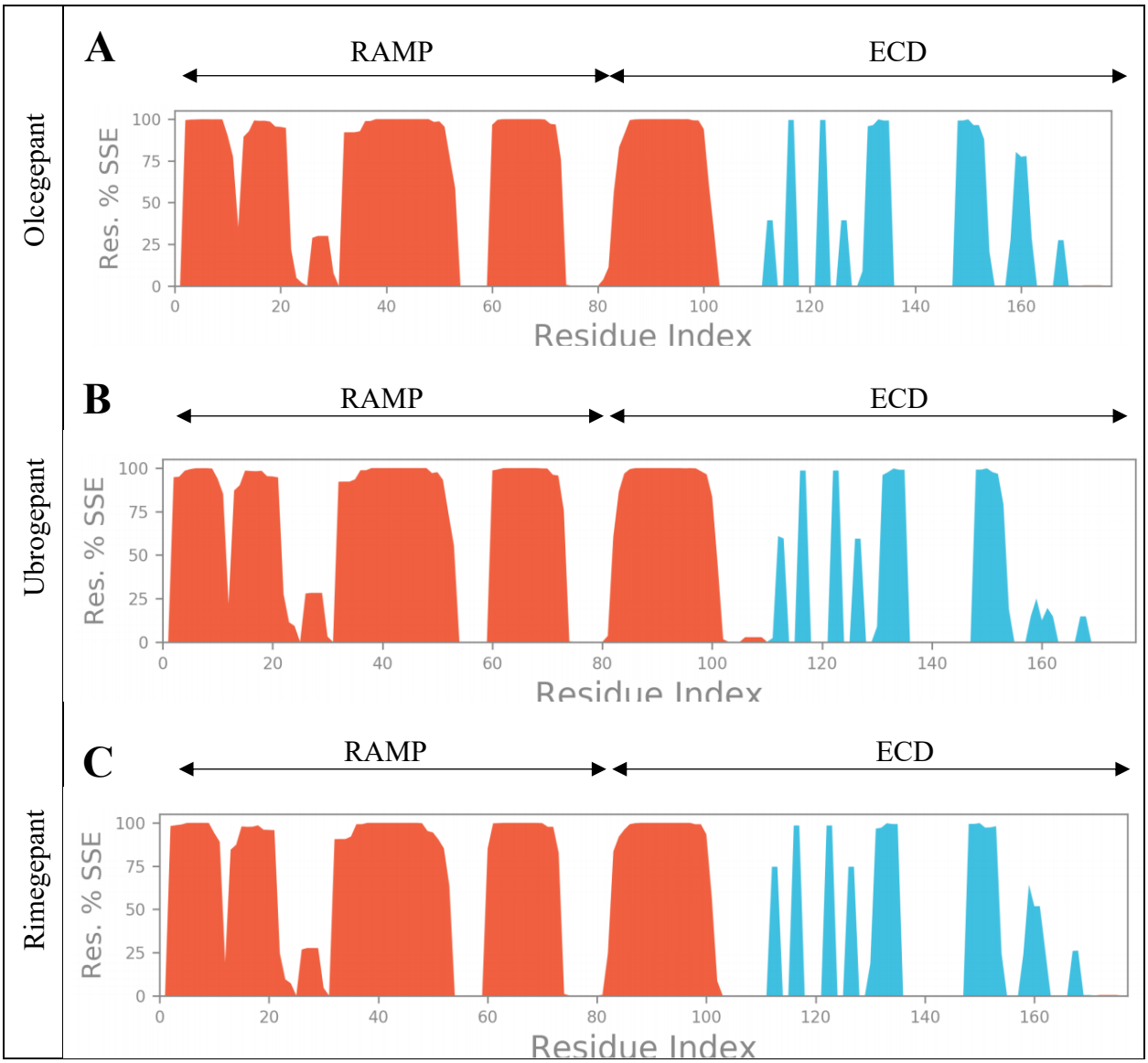

Figure 6. Protein Secondary Structure elements for three systems. Orange represents alpha helices and blue represents beta sheets.

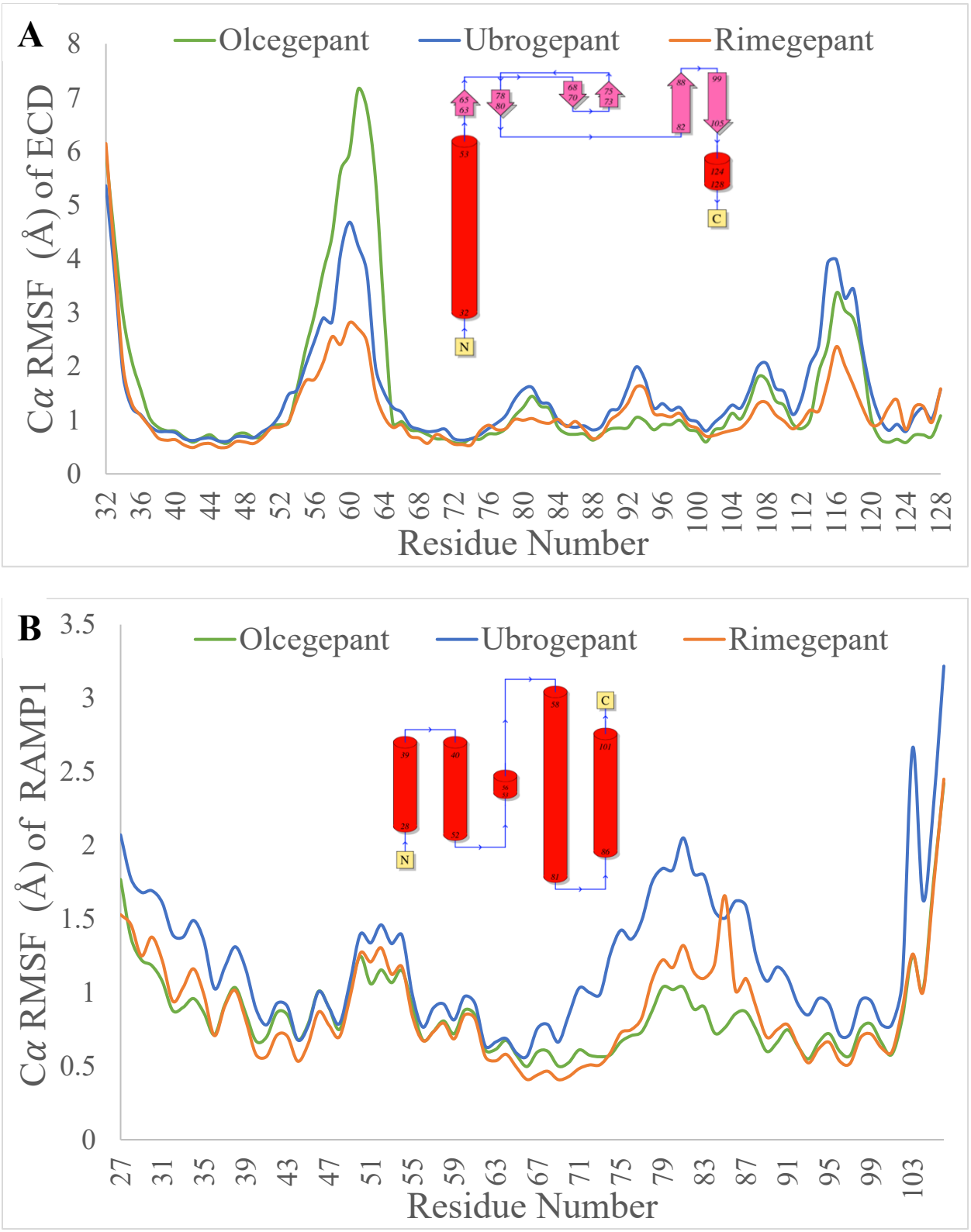

Figure 7. Protein RMSF of the Cα during MD simulation. Protein structure split into ECD (**A**) and RAMP1 (**B**) for comparison. 2D domain pictorials from PDBSum.

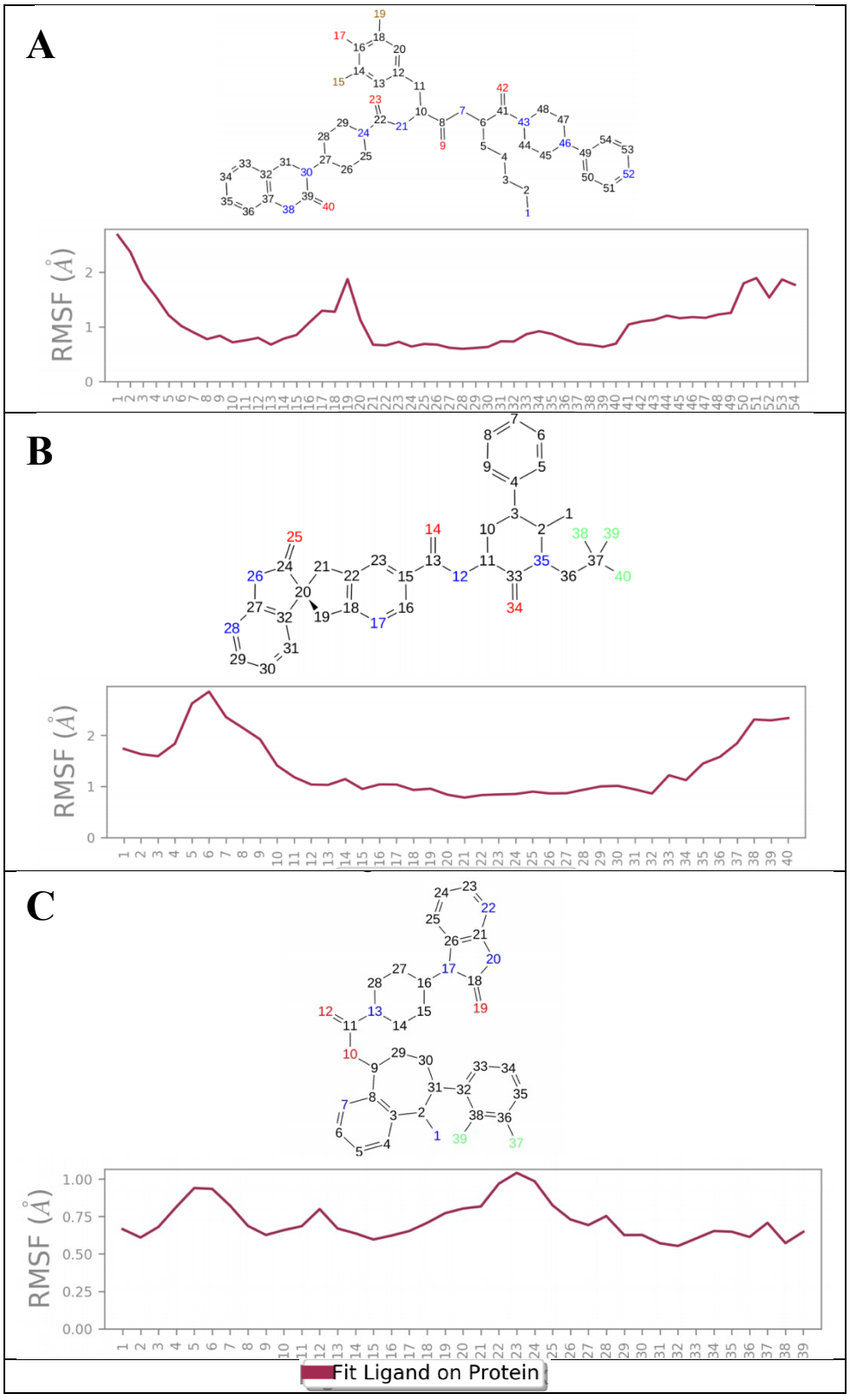

Figure 8. Ligand RMSF diagram of ECD/RAMP1 receptor with **A:** olcegepant, **B:** ubrogepant, and **C:** rimegepant.

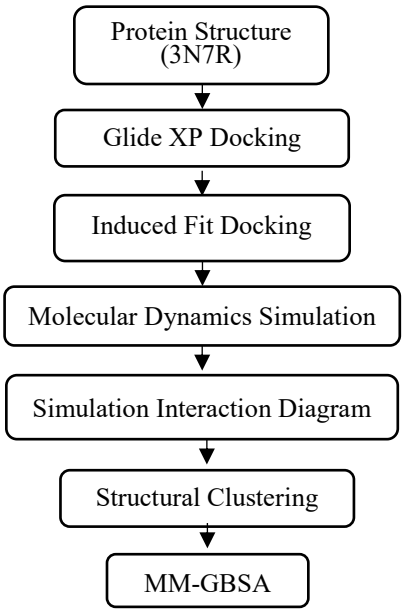

Figure 9. Workflow of analyzing binding interactions of two FDA newly approved antagonists.

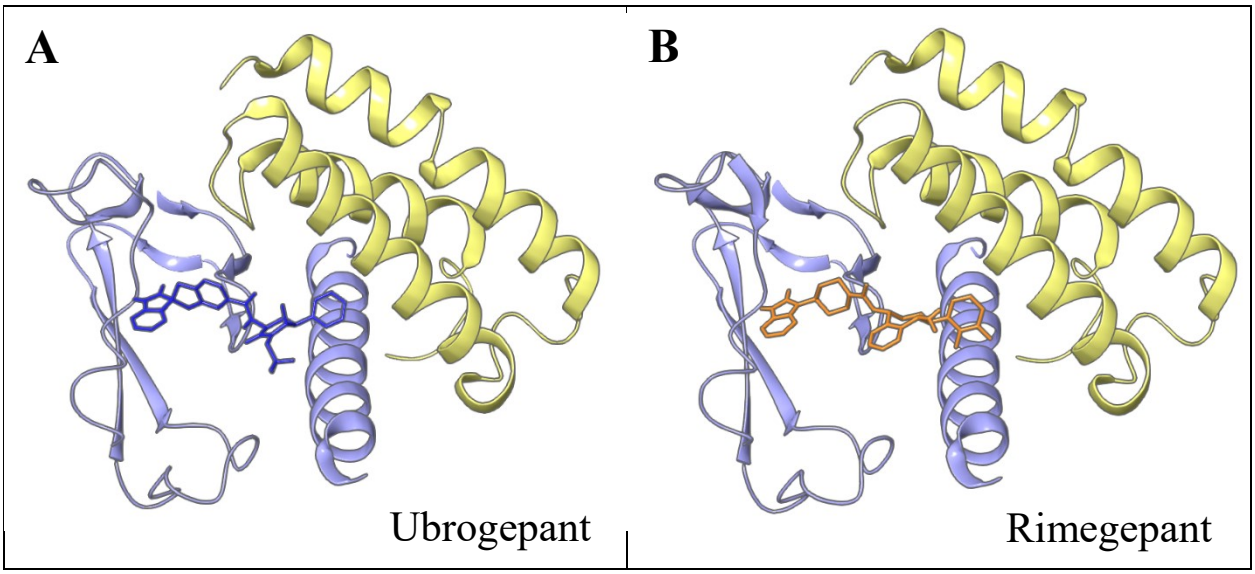

Figure 10. Best pose from IFD for two newly approved drugs. These structures are used as the initial conformation for molecular dynamics simulation. Purple ribbons represent ECD, yellow ribbons represent RAMP1.

TOC